



1 Observed and CMIP6 model simulated organic aerosol response 2 to drought in the contiguous United States during summertime

3 Wei Li^{1,2} and Yuxuan Wang¹

4 ¹Department of Earth and Atmospheric Sciences, University of Houston, Houston, Texas, USA

5 ²Now at Cooperative Institute for Satellite Earth System Studies, George Mason University, Fairfax, Virginia, USA

6 *Corresponding author: Yuxuan Wang (ywang246@central.uh.edu)*

7 **Abstract.** Drought events have been linked with the enhancements of organic aerosols (OA), but the mechanisms
8 have not been comprehensively understood. This study investigates the relationships between the monthly
9 standardized precipitation–evapotranspiration index (SPEI) and surface OA in the contiguous United States
10 (CONUS) during the summertime from 1998 to 2019. OA under severe drought conditions shows a significant
11 increase in mass concentrations across most of the CONUS relative to non-drought periods with the Pacific
12 Northwest (PNW) and Southeastern United States (SEUS) experiencing the highest average enhancement of
13 $1.79 \mu\text{g m}^{-3}$ (112 %) and $0.92 \mu\text{g m}^{-3}$ (33 %), respectively. In the SEUS, a linear regression approach between OA
14 and sulfate was used to estimate the isoprene epoxydiols derived secondary organic aerosol (IEPOX SOA), which is
15 the primary driver of the OA enhancements under droughts due to the simultaneous increase of isoprene and sulfate.
16 The rise of sulfate is mainly caused by the reduced wet deposition because of the up to 62% lower precipitation
17 amount. In the PNW, OA enhancements are closely linked to intensified wildfire emissions, which raise OA mass
18 concentrations to be four to eight times higher relative to non-fire conditions. All ten Earth system models
19 participating in the sixth phase of the Coupled Model Intercomparison Project (CMIP6) can capture the negative
20 slopes between SPEI and OA in the PNW with CESM2-WACCM and GFDL-ESM4 performing the best and worst
21 in predicting the OA enhancement under severe droughts. However, all models significantly underestimate the OA
22 increase in the SEUS with Nor-ESM2-LM and MIRCO6 showing relatively better performance. This study reveals
23 the key drivers of the elevated OA levels under droughts in the CONUS and underscores the deficiencies of current
24 climate models in their predictive capacity for assessing the impact of future droughts on air quality.

25 1. Introduction

26 Drought events, marked by prolonged periods of water scarcity and precipitation deficits, have profound impacts on
27 the hydrological cycle, ecosystems, and society (Wilhite et al., 2007). The contiguous United States (CONUS) is
28 especially prone to droughts, and recent years have witnessed an escalation in both the frequency and severity of
29 drought episodes across various regions (Strzepek et al., 2010; Leeper et al., 2022). These drought events are
30 intricately linked to the modifications in atmospheric processes, such as emission, production, transport, and
31 deposition, which can extend beyond the immediate hydrological impacts with far-reaching implications for air
32 quality. Specifically, organic aerosol (OA), a major component of the particulate matter with an aerodynamic



33 diameter less than or equal to 2.5 μm ($\text{PM}_{2.5}$), emerges as a critical air quality concern influenced by the complex
34 interactions between drought-induced meteorological conditions and biogeochemical processes.

35 OA can be directly emitted into the atmosphere through combustion activities, such as transportation fuel and
36 biomass burning. This kind of OA is called primary organic aerosol (POA), whereas secondary organic aerosol
37 (SOA) is produced by the oxidation of volatile organic compounds (VOCs). The intricate interplay between drought
38 and OA dynamics involves complex feedback mechanisms. Biogenic isoprene, mainly emitted by terrestrial
39 vegetation, is an important precursor of SOA and is highly sensitive to drought conditions. Both laboratory and field
40 measurements have shown that biogenic emissions of isoprene will increase at the initial stage of drought
41 development primarily due to temperature stimulus but drop eventually under prolonged severe drought limited by
42 soil water availability (Pegoraro et al., 2005; Brilli et al., 2007; Potosnak et al., 2014). The abnormally high
43 temperature and low humidity under droughts can enhance the volatility and oxidation of OA (Maria et al., 2004;
44 Yli-Juuti et al., 2021), while low cloud water content lowers the aqueous SOA formation (Brégonzio-Rozier et al.,
45 2016; Tsui et al., 2019), leading to compensating changes in the mass and hygroscopicity of OA. Aerosols are most
46 effectively removed by wet scavenging, which will be reduced under lower rainfall intensity and frequency (Dawson
47 et al., 2007; Fang et al., 2011). In addition, dry conditions can trigger large and high-intensity wildfires, emitting
48 more OA to the atmosphere (Taufik et al., 2017; Ruffault et al., 2018). The interactions of these factors underscore
49 the need for a comprehensive understanding of the mechanisms driving variations in OA during drought events.

50 OA, due to its fine particulate nature and diverse chemical composition, exerts significant adverse effects on climate
51 and human health. Exposure to SOA is associated with a 6.5 times higher mortality rate in the CONUS than total
52 $\text{PM}_{2.5}$ mass (Pye et al., 2021). OA can scatter solar radiation, form cloud condensation nuclei, and affect cloud
53 droplet concentrations, posing big uncertainties on radiative forcing and climate feedback (Carslaw et al., 2013; Lee
54 et al., 2016). The coupled chemistry-climate models and Earth system models (ESMs) are fundamental tools for
55 studying global warming and the accuracy of OA simulations in these models are crucial constraints on their
56 credibility in climate change simulation and projection (Thornhill et al., 2021; Gomez et al., 2023). The Coupled
57 Model Intercomparison Project Phase 6 (CMIP6), containing the new generation of ESMs with interactive aerosol
58 and gas chemistry implemented (Turnock et al., 2020), provides a valuable opportunity to evaluate the simulated OA
59 and its response to drought, which is projected to be more frequent in the future (Cook et al., 2018)

60 Several case studies have focused on the impacts of droughts on the concentrations and speciation of $\text{PM}_{2.5}$ in the
61 CONUS by calculating the differences between drought and non-drought years (Wang et al., 2015; Borlina and
62 Rennó, 2017; Zhao et al., 2019). Wang et al. (2015) and Zhao et al. (2019) compared the concentrations of $\text{PM}_{2.5}$
63 and its compositions in the southern/southeastern U.S. during the severe drought in the 2011 summertime against the
64 non-drought year of 2010 and 2013, respectively. They show that $\text{PM}_{2.5}$ has a respective enhancement of 47% and
65 65% with the largest contribution from the increase of organic carbon (OC) by 119% and 117%. Following OC,
66 sulfate in the southeast US is enhanced by 84% during the 2011 drought relative to 2013. However, fewer studies
67 have carried out long-term analyses, which can help derive a more robust drought-aerosol association than case



68 studies. Wang et al. (2017) performed a 25-year analysis during the growing season (March-October) from 1990 to
69 2014 and found that, on a monthly scale, the overall 17% enhancement of PM_{2.5} in the CONUS is mainly attributed
70 to the increase of OA, sulfate, and dust. Each of these species has a unique spatial pattern in their response to
71 droughts, which warrants a further subregional analysis to reveal the processes causing such spatial distribution
72 discrepancy.

73 In this study, we focus on the changes in OA under droughts over the CONUS during the study period of
74 summertime from 1998 to 2019. Spatial patterns of the responses of OA to droughts will be explored, followed by a
75 regional analysis focusing on the southeastern US (SEUS) and Pacific Northwest (PNW) where the highest
76 responsive rates of OA to droughts are found. The processes responsible for the increase of OA in these regions will
77 be discussed. At last, the observed drought-OA relationships will be used as a process-level metric to evaluate OA
78 simulations in the CMIP6 ESMs, which can shed light on future model development and improve aerosol
79 predictions.

80 **2. Datasets**

81 **2.1 Drought indicator**

82 The one-month gridded Standardized Precipitation-Evapotranspiration Index (SPEI) data from the global SPEI
83 database (<https://spei.csic.es/>, last access: November 27, 2023) was selected as the drought indicator because of its
84 numerical nature allowing for statistical analysis (e.g., correlation and regression). The SPEI is a multi-scaler index,
85 allowing for the identification and comparison of drought severity through time and space (Vicente-Serrano et al.,
86 2010). Negative values of SPEI are indicative of droughts and vice versa. The dataset has a spatial resolution of 0.5°
87 × 0.5° and a temporal range of 1973-2018. A composite analysis can also be conducted by applying the criteria of
88 SPEI < -1.3 and SPEI > -0.5 to denote severe drought and non-drought conditions, respectively, as suggested by Wang
89 et al. (2017).

90 **2.2 Air quality and meteorological data**

91 To expand the spatial coverage, we created a gridded daily organic carbon (OC) dataset (0.5° × 0.5°) from 1998 to
92 2018 that aggregates site-based observations from the Interagency Monitoring of Protected Visual Environments
93 (IMPROVE) network using the modified inverse distance weighting method as done by Schnell et al. (2014). Data
94 from the IMPROVE sites has been widely used by previous studies to investigate surface particulate matter trends or
95 variations in the CONUS (e.g., Hand et al., 2012). A factor of 2.1 was used to convert OC observations to OA as
96 suggested by other studies (Pye et al., 2017; Schroder et al., 2018). US Environmental Protection Agency Chemical
97 Speciation Network (EPA-CSN) also provides long-term OA data, but the CSN network uses different sampling
98 practices and analytical methods from IMPROVE, which can lead to systematic differences in OA measurements
99 (Hand et al., 2012; Gorham et al., 2021). Thus, we only used the IMPROVE dataset in this study. To reduce the artifact
100 caused by different data completeness (e.g., old sites retired and new sites started), we selected the sites with data
101 records longer than 5 years during the study period for interpolation following Li and Wang (2022).



102 Sulfate is known to influence the formation of isoprene epoxydiols derived secondary organic aerosol (IEPOX SOA),
103 a key component of OA. To explore how this linkage changes with drought, we generated a gridded sulfate dataset
104 following the same method as OC. Monthly sulfate wet depositions with associated precipitation amount and pH were
105 obtained from the National Atmospheric Deposition Program (NADP). There is a total of 53 NADP sites in the SEUS
106 (defined in Section 3.1) with a more than 5-year data record during the study period. We obtained the satellite-based
107 low level (below 700 hPa) cloud cover and liquid water content (LWC) between 2000 to 2018 from the Clouds and
108 the Earth's Radiant Energy System (CERES) monthly Single Scanner Footprint $1^\circ \times 1^\circ$ (SSF1deg) product
109 (https://asdc.larc.nasa.gov/project/CERES/CER_SSF1deg-Month_Terra-MODIS_Edition4A, last access: November
110 28, 2023). To investigate OA changes from wildfire, monthly open fire emissions were from the Global Fire Emission
111 Database version 4 (GFED4) for 1998–2018 (Giglio et al., 2013).

112 2.3 CMIP6 AerChemMIP models

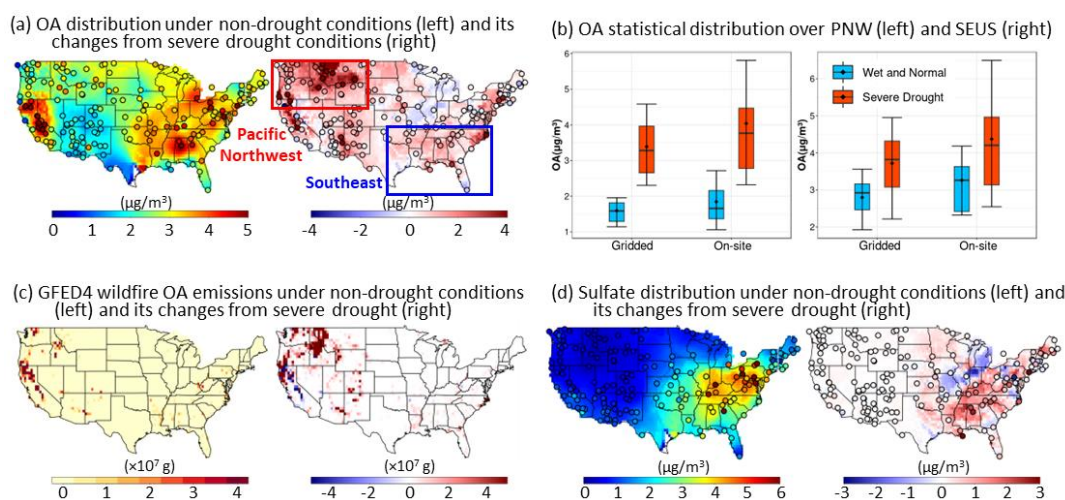
113 Ten models from the CMIP6 Aerosol Chemistry Model Intercomparison Project (AerChemMIP) were selected: BCC-
114 ESM1, CESM2-WACCM, CNRM-ESM2-1, EC-Earth3-AerChem, GFDL-ESM4, GISS-E2-1-G, MIROC6, MRI-
115 ESM2-0, NorESM2-LM, and UKESM1-0-LL. They are the only models found by the time of writing with OA and
116 sulfate mass concentration outputs from historical simulations with prescribed sea surface temperature in the
117 AerChemMIP project from 1850 to 2014. No ensemble members were found for the ten models. Various aerosol
118 schemes are used by the models with different treatments for gas phase reactions, secondary aerosol formation, and
119 aerosol-cloud interactions. More information and references (Dunne et al., 2020; Kelley et al., 2020; Séférian et al.,
120 2019; Yukimoto et al., 2019; Wu et al., 2020; Danabasoglu et al., 2020; van Noije et al., 2021; Tatebe et al., 2019;
121 Seland et al., 2020; Senior et al., 2020) for each model are listed in Table S1.

122 3. Results

123 3.1 Spatial Distributions of Organic Aerosol Response to Drought

124 Figure 1a shows the maps of the mean summertime (JJA 1998–2018) surface OA concentrations under non-drought
125 conditions and their changes under severe droughts with the observational sites (dots) overlaid. Higher
126 concentrations can be found in central California and the eastern US under non-drought conditions, reflecting the
127 average spatial distributions of summertime OA. Under severe droughts, most of the grids and sites display an
128 enhanced OA level with a mean increase of $0.72 \mu\text{g m}^{-3}$ across all the grids and $0.78 \mu\text{g m}^{-3}$ across all the sites in
129 the CONUS. Higher enhancements occur in the Pacific Northwest (PNW; red box) and southeast U.S. (SEUS; blue
130 box). In both regions, the overall gridded OA statistical distributions under severe droughts move towards the higher
131 end compared with those under non-drought conditions (Figure 1b), with an increase in the mean value by
132 $1.79 \mu\text{g m}^{-3}$ (112 %) and $0.92 \mu\text{g m}^{-3}$ (33 %) across the PNW and SEUS, respectively. Similar results are found
133 using on-site data with a respective increase of mean value by $2.18 \mu\text{g m}^{-3}$ (118 %) and $1.11 \mu\text{g m}^{-3}$ (34 %), which
134 indicates the interpolation does not significantly affect the results.

135



136

137

138

139

140

141

Figure 1. (a) Maps of the mean gridded and in situ (dots) OA under non-drought (wet and normal) conditions (left) from 1998 to 2019 in JJA and its changes from severe drought conditions (right). (b) Comparisons of statistical distributions of gridded and on-site OA mass concentrations under severe drought (red boxes) and non-drought (blue boxes) conditions over the Pacific Northwest (left) and southeast region (right). (c-d) Same as a, but for OA monthly wildfire emissions from GFED4 inventory and sulfate, respectively.

142

143

144

145

146

147

148

149

150

151

152

153

154

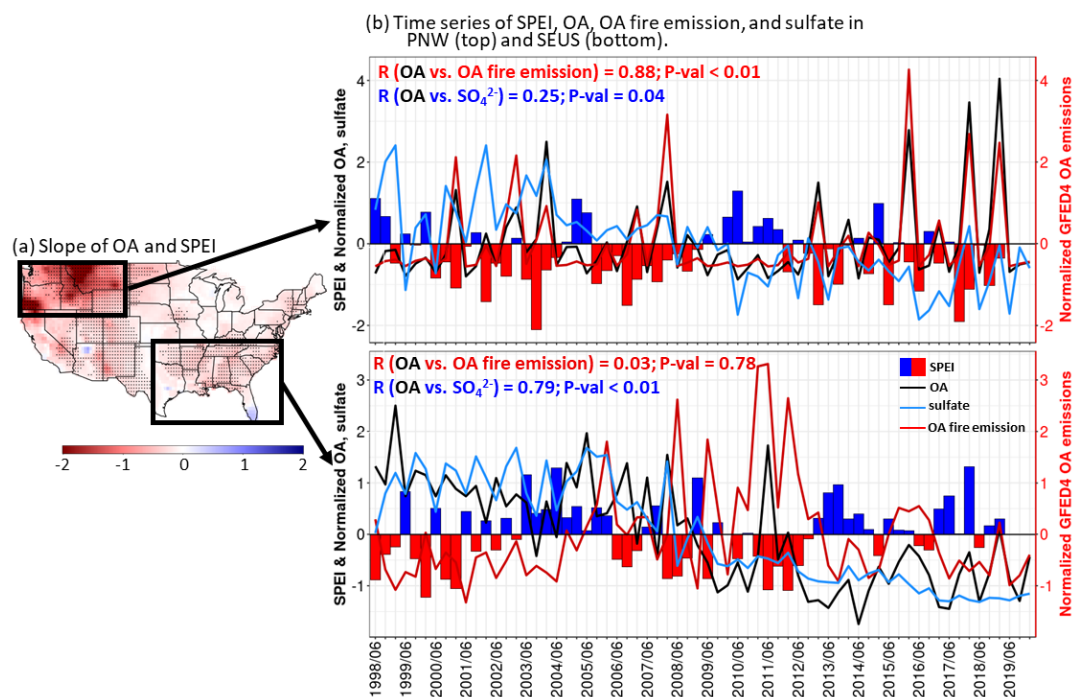
155

156

157

158

Wildfire, a major source of biomass burning, is one of the biggest contributors to both POA and SOA globally (Hallquist et al., 2009; Gilman et al., 2015; Jen et al., 2019). In the western U.S., OA, as the largest component of $\text{PM}_{2.5}$, experiences an upward trend, opposite to the rest of the country, due to the increasingly higher wildfire frequency (Dennison et al., 2014; McClure & Jaffe, 2018; Wang, et al., 2022). Indeed, we found many ‘hot spots’ of wildfire emissions of OA over the western U.S. under non-drought conditions based on the GFED4 wildfire fire inventory (Figure 1c). Severe droughts can lead to extremely high wildfire OA emissions over the PNW region, which corresponds to the highest OA enhancement as shown in Figure 1a. In contrast, the SEUS undergoes a much lower enhancement of wildfire OA emissions under severe droughts. Biogenic secondary organic aerosol (BSOA) is reported to be the major fine aerosol component in the SEUS, accounting for 60%–90% of the total $\text{PM}_{2.5}$, due to the abundant isoprene emissions (Zhang et al., 2012; Hidy et al., 2014; Kim et al., 2015). The concentrations of BSOA in the SEUS region strongly depend on ambient sulfate through the reactive uptake of gas-phase isoprene epoxydiols (IEPOX) onto the aqueous acidified surface of sulfate particles (Surratt et al., 2010; Xu et al., 2015; Lopez-Hilfiker et al., 2016; Malm et al., 2017). Interestingly, the highest sulfate increase during drought is found in the SEUS (Figure 1d), presumably due to enhanced gas-phase sulfate production and reduced wet deposition (Wang et al., 2015; Xie et al., 2019). The higher sulfate concentrations during droughts lead to the enhanced formation of IEPOX SOA, which is likely an important factor leading to a higher OA level in the SEUS.



159

160 **Figure 2. (a) Map of the slopes between monthly gridded OA and SPEI. Black dots indicate the slopes with P-values less than**
161 **0.05. (b) Time series of SPEI (bar), normalized OA (black line), sulfate (blue line), and wildfire OA emissions from GFED4**
162 **inventory (red line; right axis) averaged across the PNW (top) and SEUS (bottom) region. The numbers indicate the**
163 **correlation coefficient (R) and P-value (P-val) between OA and sulfate (blue) and wildfire emissions (red).**

164

165 Using the numerical drought indicator of SPEI, we calculated the linear slopes between monthly OA and SPEI in
166 each grid (Figure 2a). Consistent with the composite analysis in Figure 1a, most of the grids show negative slopes
167 with the highest absolute values of more than $2 \mu\text{g m}^{-3}$ per unit change of SPEI occurring in the PNW region. Since
168 negative values of SPEI indicate droughts, the negative slopes signify an enhanced OA level over most of the
169 CONUS during drought. We further examined the monthly time series of the regional mean of SPEI, normalized
170 OA, sulfate, and OA wildfire emissions in the PNW and SEUS (Figure 2b). OA in the PNW region is strongly
171 correlated with OA emissions from fire with a high correlation coefficient (R) of 0.88. The extremely high values of
172 OA and OA fire emissions are also concurrent with droughts when SPEI is negative (red bars). On the contrary,
173 SEUS has a weak correlation between OA and OA fire emissions yet a high association between OA and sulfate
174 with an R value of 0.79. Wildfire seems only to have high contributions to peak OA values in extreme drought
175 years, such as in 2011. Based on the correlation coefficients, more than 60% and 70% of the monthly OA variability
176 can be explained by sulfate and wildfire emissions in the SEUS and PNW regions, respectively, which deserves an
177 in-depth exploration in the next section.

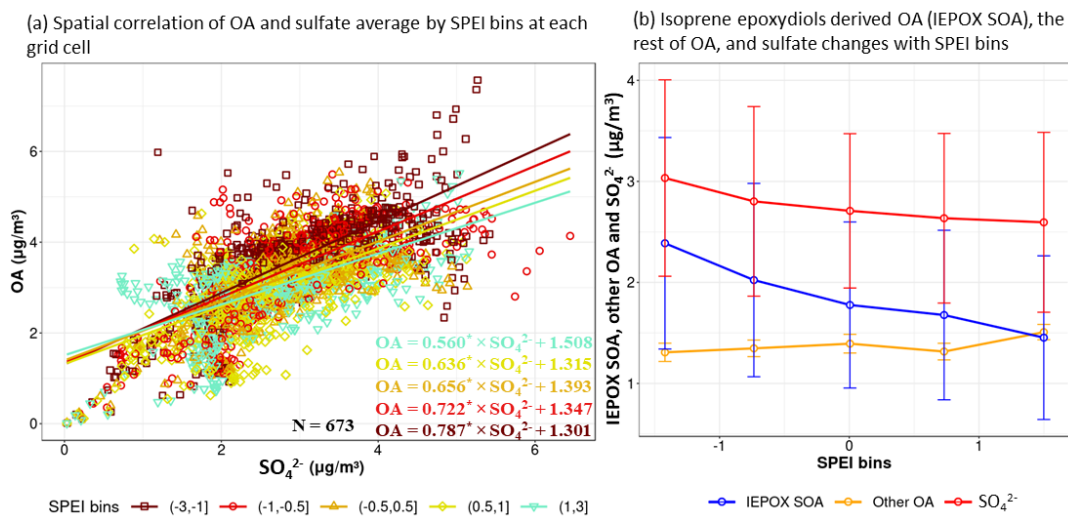
178



179 **3.2 Regional Analysis in the Pacific Northwest and Southeast US**

180 In this section, we conducted a regional analysis of OA, focusing on OA relationships with sulfate in the SEUS and
 181 with wildfire emissions in the PNW. In the SEUS, we calculated the linear regression between OA and sulfate in
 182 Figure 3a following the method of Malm et al. (2017). Each data point represents the SPEI bin-averaged value of
 183 OA and sulfate from each grid cell. The bins are divided to have approximately the same number of samples
 184 following Xie et al (2019). Only the grids with all five SPEI bins present are used (N=673), which include more than
 185 95% of the total grids (687). Thus, the binned regression calculation can represent the regional conditions of each
 186 SPEI bin. The resulting linear lines and formula are also displayed in Figure 3a. As SPEI changes from positive
 187 (non-drought) to negative (drought), the slope between OA and sulfate becomes increasingly higher, ranging from
 188 0.56 to 0.79. This indicates more OA formations per unit increase in sulfate as drought deteriorates. The higher
 189 sensitivities of OA to sulfate under droughts can be explained by increasingly higher isoprene concentrations as
 190 shown in our previous studies in the SEUS (Wang et al., 2022b; Li et al., 2022), resulting in more IEPOX in the
 191 atmosphere to be further converted to particle phase catalyzed by sulfate.

192

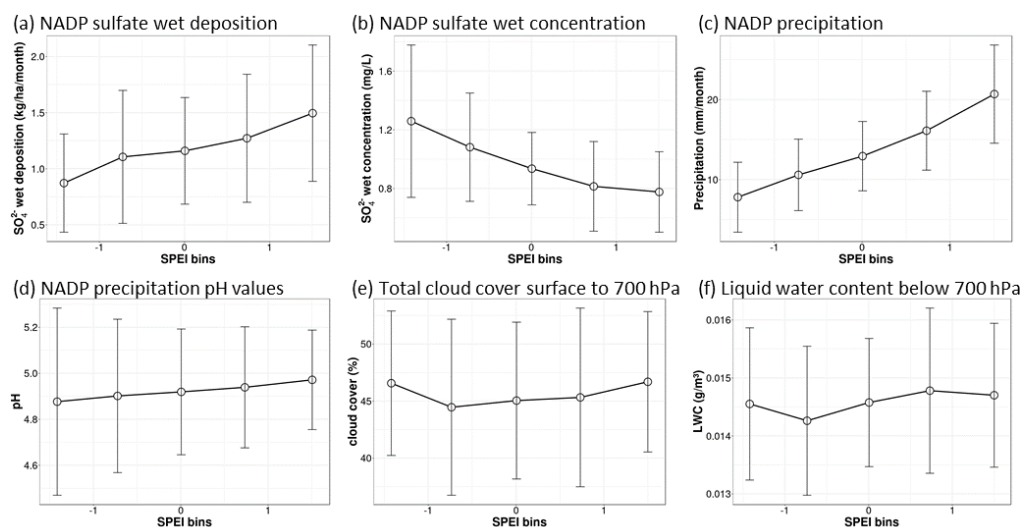


193
 194 **Figure 3. (a) Scatter plot of the SPEI bin-averaged sulfate and OA at each grid in the SEUS with solid lines representing**
 195 **the linear regressions of OA and sulfate. The corresponding linear formula of each SPEI bin is listed in the bottom-right**
 196 **corner with N indicating the number of data points for each regression calculation. The star marks in the formula indicate**
 197 **the regression significance at a 95% confidence level. (b) The isoprene epoxydiols derived SOA (IEPOX SOA), other SOA,**
 198 **and sulfate changes with SPEI derived from the linear regressions in a. Vertical bars indicate one standard deviation.**

199 The intercept of the linear regression can be interpreted as other OA components that are not associated with sulfate-
 200 catalyzed IEPOX SOA, such as POA and anthropogenic SOA (Malm et al., 2017). Figure 3b shows that the
 201 intercepts (other OA) are stable among the five SPEI bins with a less than 0.2 μg m⁻³ (15%) difference. The
 202 differences of regional mean OA minus the intercepts can then be considered as IEPOX SOA related to sulfate. The
 203 resulting estimate of IEPOX SOA is 1.45 μg m⁻³, 1.68 μg m⁻³, 1.78 μg m⁻³, 2.02 μg m⁻³ and 2.39 μg m⁻³ for the five



204 SPEI bins ranging from wet to dry conditions. These values correspond to an increase of $0.30 \mu\text{g m}^{-3}$ IEPOX SOA
 205 per unit decrease in SPEI. Interestingly, there is also an increasingly higher sulfate level from wet to dry SPEI bins
 206 with a mean value of $2.59 \mu\text{g m}^{-3}$, $2.63 \mu\text{g m}^{-3}$, $2.71 \mu\text{g m}^{-3}$, $2.80 \mu\text{g m}^{-3}$ and $3.03 \mu\text{g m}^{-3}$, respectively,
 207 corresponding to an overall increase rate of $0.14 \mu\text{g m}^{-3}$ sulfate per unit decrease of SPEI. Therefore, the increase of
 208 OA in the SEUS under droughts is largely caused by the boosted formation of BSOA due to the concurrent increase
 209 of isoprene and sulfate. This is consistent with the modeling case study by Zhao et al. (2019) who found that 98% of
 210 the SOA increase during drought in the SEUS is of biogenic origin. It is noted that the approximation of IEPOX
 211 SOA here is the upper limit of BSOA since other processes that can lead to the simultaneous changes of sulfate and
 212 OA, such as wildfire, are miscounted as BSOA in the calculation. Further analysis is needed to attribute the changes
 213 of SOA to different sources more accurately.



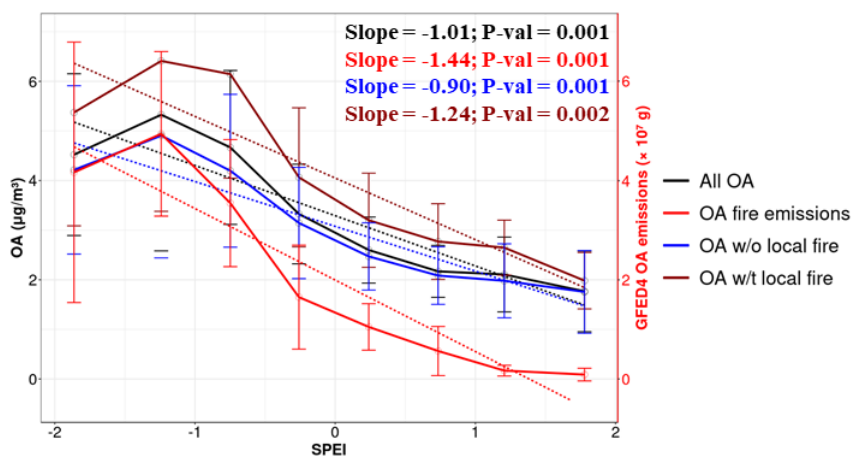
214
 215 **Figure 4. SPEI bin-averaged sulfate wet deposition (a), wet concentration (b), precipitation amount (c), precipitation pH**
 216 **values (d) from the NADP network, and the total cloud cover (e) and liquid water content (LWC; f) below 700 hPa from**
 217 **the MODIS satellite in the SEUS. Vertical bars indicate one standard deviation.**

218
 219 The source and sink of atmospheric sulfate are greatly affected by clouds and precipitation because most of the
 220 sulfate is formed in clouds and efficiently removed by wet scavenging (Barth et al., 2000; Rasch et al., 2000; Berg et
 221 al., 2015). Thus, it is understandable that sulfate is sensitive to drought considering both clouds and precipitation are
 222 significantly modulated under droughts. To further investigate the processes causing the increase of sulfate, we
 223 analyzed sulfate wet deposition, wet concentration, precipitation amount, and pH values (Figure 4a-d) from the
 224 NADP network. There is a decreasing trend of sulfate wet deposition from $1.50 \text{ kg ha}^{-1} \text{ month}^{-1}$ at the wettest (SPEI
 225 > 1) to $0.87 \text{ kg ha}^{-1} \text{ month}^{-1}$ at the driest (SPEI < -1) level. The corresponding reduction in precipitation is 62%.
 226 Since the sulfate wet deposition is calculated using sulfate wet concentration weighted by precipitation, the 50%
 227 decrease of sulfate wet deposition is driven by the reduced precipitation, which outweighs the increase of sulfate
 228 concentrations.



229 The low level (below 700 hPa) cloud cover and liquid water content (LWC) are not highly sensitive to droughts with
 230 less than 2% and 4% changes among the five SPEI bins, respectively (Figure 4e-f). Thus, the increase of sulfate wet
 231 concentrations in precipitation is likely indicative of an enhanced formation of aqueous sulfate in the clouds, which
 232 then precipitate. Alternatively, gas phase production of sulfate can also be elevated under droughts due to more
 233 sulfur dioxide (SO₂) emissions (e.g. from increased electricity generation and fires) and higher temperatures (Tai et
 234 al., 2010; Wang et al., 2017), and then washed out by rainwater droplets causing higher sulfate wet concentrations in
 235 precipitation. Either of these two pathways suggests that there is higher sulfate formation under droughts which
 236 contributes to the enhanced sulfate besides reduced wet deposition. Furthermore, the mean pH value drops steadily
 237 with dryness levels from 4.98 to 4.87, which further intensifies the acid-catalyzed IEPOX ring opening and leads to
 238 faster BSOA formation (Surratt et al., 2010).

239 Using the same approach as in the SEUS, we calculated the SPEI bin-averaged OA and OA wildfire emissions from
 240 GFED4 inventory in the PNW region shown in Figure 5. OA fire emissions grow from 0.09×10^7 g per month at the
 241 wettest level to 4.94×10^7 g per month at the second driest level (SPEI between -1.5 and -1), followed by a small
 242 drop to 4.17×10^7 g per month at the driest level (SPEI less than -1.5). This drop is likely caused by the reduction in
 243 the supply of fire fuel load under extreme drought conditions (Scasta et al., 2016). Overall, OA fire emissions
 244 increase by 1.44×10^7 g per unit decrease of SPEI per month. The mass concentrations of OA resemble the changes
 245 of OA fire emissions with an overall increase rate of $1.01 \mu\text{g m}^{-3}$ per unit decrease of SPEI, which indicates more
 246 wildfire emissions are the major driver of the higher OA concentrations in the PNW.



247 **Figure 5.** Mean (point) and one standard deviation (vertical bar) of OA (black line), wildfire OA emissions from GFED4
 248 inventory (bright red line; right axis), and OA with (dark red line) and without (blue line) local fire occurrence within each
 249 SPEI bin. The dashed lines represent the linear regression with the slopes (Slope) and P-values (P-val) of each variable
 250 listed in the top-right corner.
 251

252
 253 To better quantify the contributions of wildfire, we further separated OA values into those with local fire influences
 254 if OA fire emissions are greater than zero at each grid in each month and those without local fire influences if zero
 255 fire emissions are found. We admit that this separation relies on the accuracy of fire emissions and cannot rule out



256 the effects of the long-range transported OA from other regions, especially for the widespread drought events. As a
257 result, it may overestimate OA values with no local fire occurrence. With this caveat in mind, we calculated the
258 local fire effects as the difference between OA with and without fire emissions within each drought bin. Under the
259 wettest conditions, there is a minor difference of $0.23 \mu\text{g m}^{-3}$ between OA with and without local fire effects, while
260 this number becomes four to eight times higher under droughts ($\text{SPEI} < \text{zero}$). The local fire-affected OA with one
261 unit decrease of SPEI also increases by $0.34 \mu\text{g m}^{-3}$ faster than that without local fire occurrence. This illustrates the
262 considerable contributions of local wildfire emissions to the changes of OA under droughts. Other processes, such as
263 long-range transported aged OA and locally produced BSOA, may also contribute to the differences if their
264 contributions correlate with local fire emissions.

265 In summary, there is an increasing sensitivity of OA to sulfate as drought conditions worsen in the SEUS, driven by
266 heightened isoprene emissions and the subsequent formation of IEPOX SOA. Sulfate levels also rise under droughts,
267 influenced mainly by the reduced precipitation and the potentially increased aqueous and gas-phase sulfate
268 production. In the PNW, OA and OA wildfire emissions exhibit a close correlation, indicating that wildfire
269 emissions significantly drive higher OA concentrations therein.

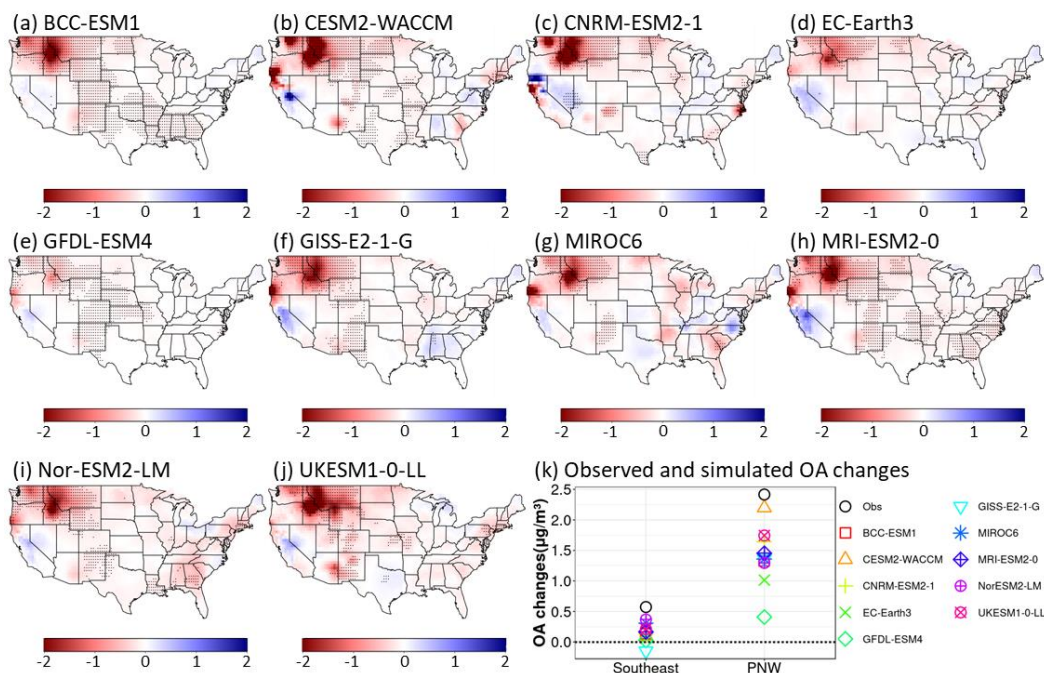
270 3.3 CMIP6 Models Simulated Organic Aerosol Response to Drought

271 In this section, we evaluated the surface OA concentrations from ten CMIP6 models regarding their capability in
272 predicting the observed SPEI-OA relationships over the CONUS during JJA 1998-2014. OA values from each
273 model were interpolated linearly to match the spatial resolution of the gridded observational dataset. Figure 6a-j
274 show the spatial distributions of the slopes between SPEI and OA simulated by each model. Compared with the
275 observed slopes in Figure 2a, all models capture the strong negative slopes of more than $2 \mu\text{g m}^{-3}$ per unit decrease
276 of SPEI in the PNW region except for GFDL-ESM4 which shows a much smaller slope of less than $1 \mu\text{g m}^{-3}$ per
277 SPEI. This indicates the CMIP6 models correctly represent the sign and magnitude of the changes in OA fire
278 emissions with droughts. By contrast, all the models have difficulties in reproducing the observed linear
279 relationships between OA and SPEI in the SEUS. Compared to the significantly negative slope from observations,
280 most of the models display insignificant or even positive slopes in the SEUS. BCC-ESM1, MRI-ESM2-0, and Nor-
281 ESM2-LM show negative slopes only in part of the SEUS grids.

282 We also evaluated model predicted average OA enhancement under severe droughts relative to non-drought periods
283 in PNW and SEUS (Figure 6k). In the PNW region, CESM2-WACCM simulates an increase of OA mass
284 concentration by $2.20 \mu\text{g m}^{-3}$, closest to the observed value of $2.41 \mu\text{g m}^{-3}$, followed by UKESM1-0-LL and
285 CNRM-ESM2-1 with an enhancement of $1.74 \mu\text{g m}^{-3}$ and $1.64 \mu\text{g m}^{-3}$, respectively. GFDL-ESM4 shows the
286 highest underestimation of the OA enhancement by $2 \mu\text{g m}^{-3}$ (83%), consistent with its smallest slopes shown in
287 Figure 6e. Smaller underestimations are found in other models, ranging from $0.96 \mu\text{g m}^{-3}$ (40%) for MRI-ESM2-0
288 to $1.4 \mu\text{g m}^{-3}$ (58%) for EC-Earth3. In the SEUS, all the ten models underpredict the observed OA increase of 0.57
289 $\mu\text{g m}^{-3}$ with the two lowest underestimations of $0.21 \mu\text{g m}^{-3}$ (37%) and $0.27 \mu\text{g m}^{-3}$ (47%) found for Nor-ESM2-LM
290 and MIRCO6, respectively. The other eight models show marginal OA enhancements between $0.02 \mu\text{g m}^{-3}$ to 0.21

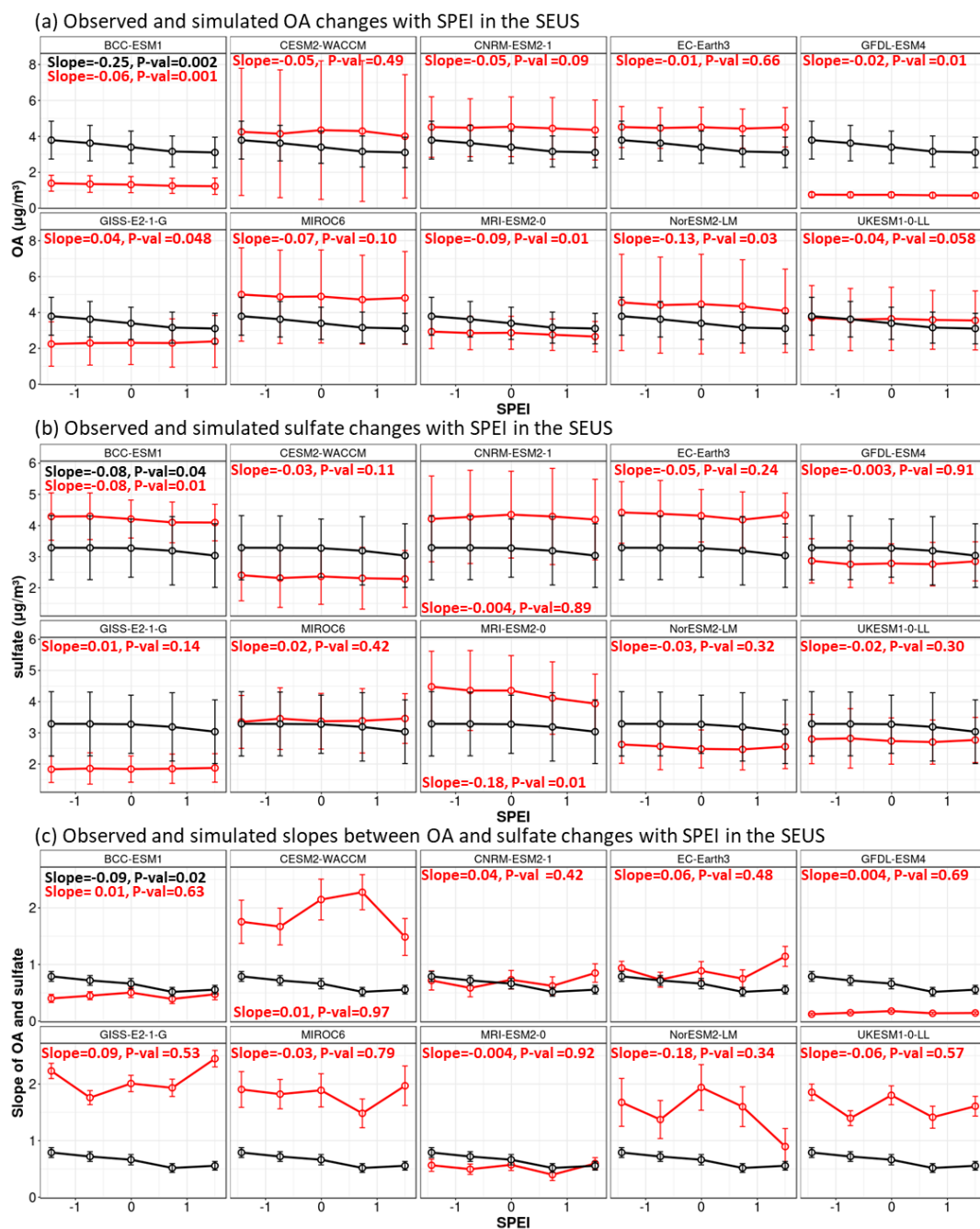


291 $\mu\text{g m}^{-3}$ or even a decrease (GISS-E2-1-G), indicating the incapacities of these models in predicting OA changes in
 292 the SEUS under droughts.



293 **Figure 6.** (a–j) Slopes between CMIP6 model simulated OA and SPEI from 1998 to 2014 during summertime with black
 294 dots indicating the P-values less than 0.05. (k) Observed and simulated OA changes under severe droughts relative to non-
 295 drought conditions during the same study period in the PNW and SEUS regions.
 296

297
 298 The poor model performance in capturing the OA changes under severe drought in the SEUS inspires us to conduct
 299 a further regional analysis following Section 3.2. The observed and simulated changes of SEUS-mean OA, sulfate,
 300 and their slopes within each SPEI bin are shown in Figure 7a-c, respectively. For the absolute OA mass
 301 concentrations, UKESM1-0-LL has the best predictions with a less than $0.5 \mu\text{g m}^{-3}$ mean bias in each SPEI bin.
 302 CESM2-WACCM, CNRM-ESM2-1, EC-Earth3, MICRO6, and NorESM2-LM overestimate OA values, while the
 303 other four models show an underestimation. For the sensitivity of OA to droughts, NorESM2-LM performs the best
 304 with an increase rate of $0.13 \mu\text{g m}^{-3}$ per unit decrease of SPEI, although the rate is only 50% of the observed value
 305 of $0.25 \mu\text{g m}^{-3}$. This is consistent with the result that this model has the lowest underestimation of OA enhancement
 306 under severe droughts. Higher underestimations of the OA sensitivity to droughts are found in MRI-ESM2-0, BCC-
 307 ESM1, and GFDL-ESM4 with a change rate of $0.09 \mu\text{g m}^{-3}$, $0.06 \mu\text{g m}^{-3}$ and $0.02 \mu\text{g m}^{-3}$ per SPEI. On the contrary,
 308 GISS-E2-1-G simulates a decrease in OA by $0.04 \mu\text{g m}^{-3}$ per unit decrease of SPEI, which is consistent with the
 309 negative OA changes under severe droughts. The rest of the models do not have a statistically significant change rate
 310 of OA with droughts at a 95% confidence level.



311
 312 **Figure 7.** SPEI bin-averaged values of OA (a), sulfate (b), and slopes of OA and sulfate (c) from observations (black lines)
 313 and simulations (red lines) in the SEUS. Vertical bars indicate one standard deviation. The numbers in each subplot indicate
 314 the slopes (Slope) and P-values (P-val) of the linear regression between each variable and SPEI.



315
316 As described in Figure 3, the increase of OA under droughts in the SEUS is due to the concurrent increase of sulfate
317 and isoprene. To investigate if the models have this mechanism, we also evaluated the modelled sensitivities of
318 sulfate and the OA-sulfate slopes to SPEI. Only two models, BCC-ESM1 and MRI-ESM2-0, have statistically
319 significant increase rates of sulfate with the decrease of SPEI, despite their overestimation of $\sim 1 \mu\text{g m}^{-3}$ (30%) in
320 terms of the absolute sulfate concentrations. BCC-ESM1 predicts the same change rate as observations with a value
321 of $0.08 \mu\text{g m}^{-3}$ per unit change of SPEI, while MRI-ESM2-0 predicts a rate of $0.18 \mu\text{g m}^{-3}$, more than double the
322 observed rate. The slopes between OA and sulfate derived from these two models are also the closest to the
323 observed value of 0.53 in the two wettest SPEI bins, indicating the dependence of IEPOX SOA formation on sulfate
324 is well captured by these two models when no drought occurs. However, the slopes stay stable among SPEI bins and
325 cannot reproduce the observed increase rate of 0.09 per unit decrease of SPEI. Similarly, this feature is not captured
326 by the other eight models, although some of them show big variabilities (e.g., CESM2-WACCM and NorESM2-
327 LM). This suggests an insensitivity or a non-persistent change of biogenic isoprene in response to drought severity
328 in all models. In addition, seven out of ten models, excluding BCC-ESM1, MRI-ESM2-0, and GFDL-ESM4,
329 generally overestimate the slopes between OA and sulfate regardless of the dryness conditions, signifying an
330 overdependence of the formation of IEPOX SOA on sulfate in these models.

331 To sum up, most of the models can represent the linear relationships between OA and SPEI in the PNW region with
332 CESM2-WACCM and GFDL-ESM4 performing the best and worst in predicting the OA enhancement under severe
333 droughts. However, all the models face challenges in capturing the OA increases under droughts in the SEUS, with
334 Nor-ESM2-LM and MIRCO6 showing relatively better performance indicated by their lower underestimation of OA
335 enhancement. These challenges are mainly caused by the model deficiencies in the parameterization of the IEPOX
336 SOA dependence on sulfate and the concurrent increase pattern of isoprene and sulfate as drought deteriorates.

337 **4 Conclusions**

338 In this study, the changes in organic aerosol (OA) in response to drought in the CONUS were examined. We first
339 displayed the spatial patterns of OA under non-drought and severe drought conditions and found most of the
340 CONUS experiences an abnormally higher level of OA by an average of $0.72 \mu\text{g m}^{-3}$ relative to wet and normal
341 conditions. Regionally, the highest average increase occurs in the PNW and SEUS areas by $1.79 \mu\text{g m}^{-3}$ (112 %) and
342 $0.92 \mu\text{g m}^{-3}$ (33 %), respectively. The concurrent enhancement of wildfire OA emissions in the PNW and sulfate in
343 the SEUS provides more insights into an in-depth investigation over these two regions.

344 In the SEUS, a linear regression between OA and sulfate was applied to estimate the amount of IEPOX SOA and
345 other OA. Results from this simplified method indicate that the IEPOX SOA drives the increase of total OA from
346 wet to dry conditions while other OA stays stable. Both the increase of isoprene and sulfate under droughts lead to
347 the enhancement of IEPOX SOA. Data from the NADP network shows that up to 62% lower precipitation under
348 droughts induces slower sulfate wet deposition rates and thus leaves more sulfate in the atmosphere. Higher sulfate



349 wet concentration in the precipitation indicates more in-cloud and/or gas-phase sulfate production under droughts
350 since cloud cover and liquid content do not show a strong sensitivity to droughts.

351 In the PNW, there is an overall increase of 1.44×10^7 g in the monthly OA wildfire emissions per unit decrease of
352 SPEI, which is the main driver of the elevated OA. There is a plateau of the OA fire emissions with SPEI between -
353 1.5 and -1, followed by a drop with SPEI less than -1.5. This implies that wildfire activities are not linearly related to
354 moisture and are also limited by the availability of fuel load. Dividing OA into groups with or without local fire
355 influence, we found that local fire events can increase the OA concentrations by four to eight times relative to those
356 without fire activities. Future work is needed to further investigate the changes in OA from other sources, such as
357 long-range transported OA and BSOA, in this region.

358 The evaluation of surface OA concentrations from ten CMIP6 models provides valuable insights into their predictive
359 capabilities in capturing the observed relationships between SPEI and OA over the CONUS. All the models are
360 found to successfully capture the negative slopes in the PNW area, indicating correct sensitivities of OA wildfire
361 emissions to droughts in these models. However, deficiencies are revealed in the SEUS with most models displaying
362 insignificant or positive slopes between OA and SPEI as opposed to significantly negative slopes from observations.
363 The assessment of average OA enhancement during severe droughts relative to non-drought periods further
364 underscores the models' varying degrees of accuracy in simulating OA response to drought. In the PNW, CESM2-
365 WACCM stands out with its simulated OA increase of $2.20 \mu\text{g m}^{-3}$ being closest to the observed value of 2.41
366 $\mu\text{g m}^{-3}$, while GFDL-ESM4 exhibits the highest underestimation of OA enhancement by $2 \mu\text{g m}^{-3}$ (83%). In the
367 SEUS, all models consistently underpredict the observed OA increases, highlighting their limitations in predicting
368 OA changes in this region under drought conditions. These limitations can be mainly attributed to the insensitivities
369 of sulfate to SPEI, the inconsistent changes of isoprene under droughts, and the model deficiencies in the
370 parameterization of the IEPOX SOA dependence on inorganic sulfate.

371 This study reveals the key drivers of the enhanced OA mass concentrations in the CONUS, including higher wildfire
372 emissions and the simultaneous increase in biogenic isoprene and inorganic sulfate, which highlights the complex
373 physical and chemical processes involved in the aerosol composition changes under droughts. The discrepancies in
374 simulating OA enhancements during severe droughts underscore the need for ongoing model improvement,
375 particularly in accurately representing the emissions of biogenic isoprene, the life cycle of sulfate, and their intricate
376 interactions. Addressing these limitations will be crucial for enhancing the reliability of climate models and their
377 ability to predict the impact of future droughts on atmospheric composition and air quality in the CONUS.

378 **Data availability**

379 Monthly SPEI data is obtained from https://spei.csic.es/spei_database_2_6 (Vicente-Serrano et al., 2010).

380 Observations from the IMPROVE and NADP network are downloaded from

381 <https://views.cira.colostate.edu/fed/QueryWizard/> (FED, 2023). GFED4 wildfire emission inventory and MODIS

382 satellite cloud cover data are archived at <https://www.geo.vu.nl/~gwerf/GFED/GFED4/> (Giglio et al., 2013) and



383 https://asdc.larc.nasa.gov/project/CERES/CER_SSFIdeg-Month_Terra-MODIS_Edition4A (NASA, 2015),
384 respectively. The CMIP6 model outputs are publicly available online from the Earth System Federation Grid nodes.

385 **Competing interests**

386 The authors declare that they have no conflict of interest.

387 **Author contributions**

388 YW conceived the research idea. WL conducted the analysis. Both authors contributed to the preparation of the
389 manuscript.

390 **Acknowledgments**

391 The authors acknowledge researchers from the IMPROVE and NADP networks for making surface aerosol mass
392 and deposition observations. We thank individuals and groups from the Climatology and Climate Services
393 Laboratory for creating the SPEI dataset. The authors also thank the modeling groups participating in the CMIP6
394 AerChemMIP project for making the surface aerosol species outputs available.

395 **Financial support**

396 This research has been supported by the National Oceanic and Atmospheric Administration through the
397 Atmospheric Chemistry, Carbon Cycle and Climate (AC4) Program (grant no. NA19OAR4310177).

398 **References**

- 399 Barth, M. C., Rasch, P. J., Kiehl, J. T., Benkovitz, C. M., and Schwartz, S. E.: Sulfur chemistry in the National
400 Center for Atmospheric Research Community Climate Model: Description, evaluation, features, and sensitivity to
401 aqueous chemistry, *J. Geophys. Res. Atmospheres*, 105, 1387–1415, <https://doi.org/10.1029/1999JD900773>, 2000.
- 402 Berg, L. K., Shrivastava, M., Easter, R. C., Fast, J. D., Chapman, E. G., Liu, Y., and Ferrare, R. A.: A new WRF-
403 Chem treatment for studying regional-scale impacts of cloud processes on aerosol and trace gases in parameterized
404 cumuli, *Geosci. Model Dev.*, 8, 409–429, <https://doi.org/10.5194/gmd-8-409-2015>, 2015.
- 405 Borlina, C. S. and Rennó, N. O.: The impact of a severe drought on dust lifting in California’s Owens Lake area,
406 *Sci. Rep.*, 7, 1784, <https://doi.org/10.1038/s41598-017-01829-7>, 2017.
- 407 Brégonzio-Rozier, L., Giorio, C., Siekmann, F., Pangui, E., Morales, S. B., Temime-Roussel, B., Gratien, A.,
408 Michoud, V., Cazaunau, M., DeWitt, H. L., Tapparo, A., Monod, A., and Doussin, J.-F.: Secondary organic aerosol
409 formation from isoprene photooxidation during cloud condensation–evaporation cycles, *Atmospheric Chem. Phys.*,
410 16, 1747–1760, <https://doi.org/10.5194/acp-16-1747-2016>, 2016.
- 411 Brillì, F., Barta, C., Fortunati, A., Lerdau, M., Loreto, F., and Centritto, M.: Response of isoprene emission and
412 carbon metabolism to drought in white poplar (*Populus alba*) saplings, *New Phytol.*, 175, 244–254,
413 <https://doi.org/10.1111/j.1469-8137.2007.02094.x>, 2007.



- 414 Carslaw, K. S., Lee, L. A., Reddington, C. L., Pringle, K. J., Rap, A., Forster, P. M., Mann, G. W., Spracklen, D. V.,
415 Woodhouse, M. T., Regayre, L. A., and Pierce, J. R.: Large contribution of natural aerosols to uncertainty in indirect
416 forcing, *Nature*, 503, 67–71, <https://doi.org/10.1038/nature12674>, 2013.
- 417 Cook, B. I., Mankin, J. S., and Anchukaitis, K. J.: Climate change and drought: From past to future, *Curr. Clim.*
418 *Change Rep.*, 4, 164–179, <https://doi.org/10.1007/s40641-018-0093-2>, 2018.
- 419 Danabasoglu, G., Lamarque, J.-F., Bacmeister, J., Bailey, D. A., DuVivier, A. K., Edwards, J., Emmons, L. K.,
420 Fasullo, J., Garcia, R., Gettelman, A., Hannay, C., Holland, M. M., Large, W. G., Lauritzen, P. H., Lawrence, D. M.,
421 Lenaerts, J. T. M., Lindsay, K., Lipscomb, W. H., Mills, M. J., Neale, R., Oleson, K. W., Otto-Bliessner, B., Phillips,
422 A. S., Sacks, W., Tilmes, S., van Kampenhout, L., Versteinstein, M., Bertini, A., Dennis, J., Deser, C., Fischer, C.,
423 Fox-Kemper, B., Kay, J. E., Kinnison, D., Kushner, P. J., Larson, V. E., Long, M. C., Mickelson, S., Moore, J. K.,
424 Nienhouse, E., Polvani, L., Rasch, P. J., and Strand, W. G.: The Community Earth System Model Version 2
425 (CESM2), *J. Adv. Model. Earth Syst.*, 12, e2019MS001916, <https://doi.org/10.1029/2019MS001916>, 2020.
- 426 Dawson, J. P., Adams, P. J., and Pandis, S. N.: Sensitivity of PM_{2.5} to climate in the Eastern US: a modeling case
427 study, *Atmospheric Chem. Phys.*, 7, 4295–4309, <https://doi.org/10.5194/acp-7-4295-2007>, 2007.
- 428 Dennison, P. E., Brewer, S. C., Arnold, J. D., and Moritz, M. A.: Large wildfire trends in the western United States,
429 1984–2011, *Geophys. Res. Lett.*, 41, 2928–2933, <https://doi.org/10.1002/2014GL059576>, 2014.
- 430 Dunne, J. P., Horowitz, L. W., Adcroft, A. J., Ginoux, P., Held, I. M., John, J. G., Krasting, J. P., Malyshev, S.,
431 Naik, V., Paulot, F., Shevliakova, E., Stock, C. A., Zadeh, N., Balaji, V., Blanton, C., Dunne, K. A., Dupuis, C.,
432 Durachta, J., Dussin, R., Gauthier, P. P. G., Griffies, S. M., Guo, H., Hallberg, R. W., Harrison, M., He, J., Hurlin,
433 W., McHugh, C., Menzel, R., Milly, P. C. D., Nikonov, S., Paynter, D. J., Ploshay, J., Radhakrishnan, A., Rand, K.,
434 Reichl, B. G., Robinson, T., Schwarzkopf, D. M., Sentman, L. T., Underwood, S., Vahlenkamp, H., Winton, M.,
435 Wittenberg, A. T., Wyman, B., Zeng, Y., and Zhao, M.: The GFDL Earth System Model Version 4.1 (GFDL-ESM
436 4.1): Overall Coupled Model Description and Simulation Characteristics, *J. Adv. Model. Earth Syst.*, 12,
437 e2019MS002015, <https://doi.org/10.1029/2019MS002015>, 2020.
- 438 Fang, Y., Fiore, A. M., Horowitz, L. W., Gnanadesikan, A., Held, I., Chen, G., Vecchi, G., and Levy, H.: The
439 impacts of changing transport and precipitation on pollutant distributions in a future climate, *J. Geophys. Res.*
440 *Atmospheres*, 116, <https://doi.org/10.1029/2011JD015642>, 2011.
- 441 FED: The Federal Land Manager Environmental Database query wizard, FED,
442 <https://views.cira.colostate.edu/fed/QueryWizard/> (last access: 27 December 2023), 2023.
- 443 Giglio, L., Randerson, J. T., and van der Werf, G. R.: Analysis of daily, monthly, and annual burned area using the
444 fourth-generation global fire emissions database (GFED4), *J. Geophys. Res. Biogeosciences*, 118, 317–328,
445 <https://doi.org/10.1002/jgrg.20042>, 2013.
- 446 Gilman, J. B., Lerner, B. M., Kuster, W. C., Goldan, P. D., Warneke, C., Veres, P. R., Roberts, J. M., de Gouw, J.
447 A., Burling, I. R., and Yokelson, R. J.: Biomass burning emissions and potential air quality impacts of volatile
448 organic compounds and other trace gases from fuels common in the US, *Atmospheric Chem. Phys.*, 15, 13915–
449 13938, <https://doi.org/10.5194/acp-15-13915-2015>, 2015.
- 450 Gomez, J., Allen, R. J., Turnock, S. T., Horowitz, L. W., Tsigaridis, K., Bauer, S. E., Olivié, D., Thomson, E. S.,
451 and Ginoux, P.: The projected future degradation in air quality is caused by more abundant natural aerosols in a
452 warmer world, *Commun. Earth Environ.*, 4, 1–11, <https://doi.org/10.1038/s43247-023-00688-7>, 2023.
- 453 Gorham, K. A., Raffuse, S. M., Hyslop, N. P., and White, W. H.: Comparison of recent speciated PM_{2.5} data from
454 collocated CSN and IMPROVE measurements, *Atmos. Environ.*, 244, 117977,
455 <https://doi.org/10.1016/j.atmosenv.2020.117977>, 2021.



- 456 Hallquist, M., Wenger, J. C., Baltensperger, U., Rudich, Y., Simpson, D., Claeys, M., Dommen, J., Donahue, N. M.,
457 George, C., Goldstein, A. H., Hamilton, J. F., Herrmann, H., Hoffmann, T., Iinuma, Y., Jang, M., Jenkin, M. E.,
458 Jimenez, J. L., Kiendler-Scharr, A., Maenhaut, W., McFiggans, G., Mentel, T. F., Monod, A., Prévôt, A. S. H.,
459 Seinfeld, J. H., Surratt, J. D., Szmigielski, R., and Wildt, J.: The formation, properties and impact of secondary
460 organic aerosol: current and emerging issues, *Atmospheric Chem. Phys.*, 9, 5155–5236, [https://doi.org/10.5194/acp-](https://doi.org/10.5194/acp-9-5155-2009)
461 9-5155-2009, 2009.
- 462 Hand, J. L., Schichtel, B. A., Pitchford, M., Malm, W. C., and Frank, N. H.: Seasonal composition of remote and
463 urban fine particulate matter in the United States, *J. Geophys. Res. Atmospheres*, 117,
464 <https://doi.org/10.1029/2011JD017122>, 2012.
- 465 Hidy, G. M., Blanchard, C. L., Baumann, K., Edgerton, E., Tanenbaum, S., Shaw, S., Knipping, E., Tombach, I.,
466 Jansen, J., and Walters, J.: Chemical climatology of the southeastern United States, 1999–2013, *Atmospheric*
467 *Chem. Phys.*, 14, 11893–11914, <https://doi.org/10.5194/acp-14-11893-2014>, 2014.
- 468 Jen, C. N., Hatch, L. E., Selimovic, V., Yokelson, R. J., Weber, R., Fernandez, A. E., Kreisberg, N. M., Barsanti, K.
469 C., and Goldstein, A. H.: Speciated and total emission factors of particulate organics from burning western US
470 wildland fuels and their dependence on combustion efficiency, *Atmospheric Chem. Phys.*, 19, 1013–1026,
471 <https://doi.org/10.5194/acp-19-1013-2019>, 2019.
- 472 Kelley, M., Schmidt, G. A., Nazarenko, L. S., Bauer, S. E., Ruedy, R., Russell, G. L., Ackerman, A. S., Aleinov, I.,
473 Bauer, M., Bleck, R., Canuto, V., Cesana, G., Cheng, Y., Clune, T. L., Cook, B. I., Cruz, C. A., Del Genio, A. D.,
474 Elsaesser, G. S., Faluvegi, G., Kiang, N. Y., Kim, D., Lacis, A. A., Leboissetier, A., LeGrande, A. N., Lo, K. K.,
475 Marshall, J., Matthews, E. E., McDermid, S., Mezzuman, K., Miller, R. L., Murray, L. T., Oinas, V., Orbe, C.,
476 García-Pando, C. P., Perlwitz, J. P., Puma, M. J., Rind, D., Romanou, A., Shindell, D. T., Sun, S., Tausnev, N.,
477 Tsigaridis, K., Tselioudis, G., Weng, E., Wu, J., and Yao, M.-S.: GISS-E2.1: Configurations and Climatology, *J.*
478 *Adv. Model. Earth Syst.*, 12, e2019MS002025, <https://doi.org/10.1029/2019MS002025>, 2020.
- 479 Kim, P. S., Jacob, D. J., Fisher, J. A., Travis, K., Yu, K., Zhu, L., Yantosca, R. M., Sulprizio, M. P., Jimenez, J. L.,
480 Campuzano-Jost, P., Froyd, K. D., Liao, J., Hair, J. W., Fenn, M. A., Butler, C. F., Wagner, N. L., Gordon, T. D.,
481 Welti, A., Wennberg, P. O., Crouse, J. D., St. Clair, J. M., Teng, A. P., Millet, D. B., Schwarz, J. P., Markovic, M.
482 Z., and Perring, A. E.: Sources, seasonality, and trends of southeast US aerosol: an integrated analysis of surface,
483 aircraft, and satellite observations with the GEOS-Chem chemical transport model, *Atmospheric Chem. Phys.*, 15,
484 10411–10433, <https://doi.org/10.5194/acp-15-10411-2015>, 2015.
- 485 Lee, L. A., Reddington, C. L., and Carslaw, K. S.: On the relationship between aerosol model uncertainty and
486 radiative forcing uncertainty, *Proc. Natl. Acad. Sci.*, 113, 5820–5827, <https://doi.org/10.1073/pnas.1507050113>,
487 2016.
- 488 Leeper, R. D., Bilotta, R., Petersen, B., Stiles, C. J., Heim, R., Fuchs, B., Prat, O. P., Palecki, M., and Ansari, S.:
489 Characterizing U.S. drought over the past 20 years using the U.S. drought monitor, *Int. J. Climatol.*, 42, 6616–6630,
490 <https://doi.org/10.1002/joc.7653>, 2022.
- 491 Li, W. and Wang, Y.: Reduced surface fine dust under droughts over the southeastern United States during
492 summertime: observations and CMIP6 model simulations, *Atmospheric Chem. Phys.*, 22, 7843–7859,
493 <https://doi.org/10.5194/acp-22-7843-2022>, 2022.
- 494 Li, W., Wang, Y., Flynn, J., Griffin, R. J., Guo, F., and Schnell, J. L.: Spatial variation of surface O₃ responses to
495 drought over the contiguous United States during summertime: Role of precursor emissions and ozone chemistry, *J.*
496 *Geophys. Res. Atmospheres*, 127, e2021JD035607, <https://doi.org/10.1029/2021JD035607>, 2022.
- 497 Lopez-Hilfiker, F. D., Mohr, C., D’Ambro, E. L., Lutz, A., Riedel, T. P., Gaston, C. J., Iyer, S., Zhang, Z., Gold, A.,
498 Surratt, J. D., Lee, B. H., Kurten, T., Hu, W. W., Jimenez, J., Hallquist, M., and Thornton, J. A.: Molecular
499 composition and volatility of organic aerosol in the southeastern U.S.: Implications for IEPOX derived SOA,
500 *Environ. Sci. Technol.*, 50, 2200–2209, <https://doi.org/10.1021/acs.est.5b04769>, 2016.



- 501 Malm, W. C., Schichtel, B. A., Hand, J. L., and Collett Jr., J. L.: Concurrent temporal and spatial trends in sulfate
502 and organic mass concentrations measured in the IMPROVE monitoring program, *J. Geophys. Res. Atmospheres*,
503 122, 10,462–10,476, <https://doi.org/10.1002/2017JD026865>, 2017.
- 504 Maria, S. F., Russell, L. M., Gilles, M. K., and Myneni, S. C. B.: Organic Aerosol Growth Mechanisms and Their
505 Climate-Forcing Implications, *Science*, 306, 1921–1924, <https://doi.org/10.1126/science.1103491>, 2004.
- 506 McClure, C. D. and Jaffe, D. A.: US particulate matter air quality improves except in wildfire-prone areas, *Proc.*
507 *Natl. Acad. Sci.*, 115, 7901–7906, <https://doi.org/10.1073/pnas.1804353115>, 2018.
- 508 NASA: CERES Time-Interpolated TOA Fluxes, Clouds and Aerosols Monthly Terra Edition4A, NASA Langley
509 Atmospheric Science Data Center DAAC [data set],
510 https://doi.org/10.5067/TERRA/CERES/SSF1DEGMONTH_L3.004A, 2015.
- 511 van Noije, T., Bergman, T., Le Sager, P., O'Donnell, D., Makkonen, R., Gonçalves-Ageitos, M., Döscher, R.,
512 Fladrich, U., von Hardenberg, J., Keskinen, J.-P., Korhonen, H., Laakso, A., Myriokefalitakis, S., Ollinaho, P., Pérez
513 García-Pando, C., Reerink, T., Schrödner, R., Wyser, K., and Yang, S.: EC-Earth3-AerChem: a global climate
514 model with interactive aerosols and atmospheric chemistry participating in CMIP6, *Geosci. Model Dev.*, 14, 5637–
515 5668, <https://doi.org/10.5194/gmd-14-5637-2021>, 2021.
- 516 Pegoraro, E., Rey, A., Barron-Gafford, G., Monson, R., Malhi, Y., and Murthy, R.: The interacting effects of
517 elevated atmospheric CO₂ concentration, drought and leaf-to-air vapour pressure deficit on ecosystem isoprene
518 fluxes, *Oecologia*, 146, 120–129, <https://doi.org/10.1007/s00442-005-0166-5>, 2005.
- 519 Potosnak, M. J., LeSturgeon, L., Pallardy, S. G., Hosman, K. P., Gu, L., Karl, T., Geron, C., and Guenther, A. B.:
520 Observed and modeled ecosystem isoprene fluxes from an oak-dominated temperate forest and the influence of
521 drought stress, *Atmos. Environ.*, 84, 314–322, <https://doi.org/10.1016/j.atmosenv.2013.11.055>, 2014.
- 522 Pye, H. O. T., Murphy, B. N., Xu, L., Ng, N. L., Carlton, A. G., Guo, H., Weber, R., Vasilakos, P., Appel, K. W.,
523 Budisulistiorini, S. H., Surratt, J. D., Nenes, A., Hu, W., Jimenez, J. L., Isaacman-VanWertz, G., Misztal, P. K., and
524 Goldstein, A. H.: On the implications of aerosol liquid water and phase separation for organic aerosol mass,
525 *Atmospheric Chem. Phys.*, 17, 343–369, <https://doi.org/10.5194/acp-17-343-2017>, 2017.
- 526 Pye, H. O. T., Ward-Caviness, C. K., Murphy, B. N., Appel, K. W., and Seltzer, K. M.: Secondary organic aerosol
527 association with cardiorespiratory disease mortality in the United States, *Nat. Commun.*, 12, 7215,
528 <https://doi.org/10.1038/s41467-021-27484-1>, 2021.
- 529 Rasch, P. J., Barth, M. C., Kiehl, J. T., Schwartz, S. E., and Benkovitz, C. M.: A description of the global sulfur
530 cycle and its controlling processes in the National Center for Atmospheric Research Community Climate Model,
531 Version 3, *J. Geophys. Res. Atmospheres*, 105, 1367–1385, <https://doi.org/10.1029/1999JD900777>, 2000.
- 532 Ruffault, J., Curt, T., Martin-StPaul, N. K., Moron, V., and Trigo, R. M.: Extreme wildfire events are linked to
533 global-change-type droughts in the northern Mediterranean, *Nat. Hazards Earth Syst. Sci.*, 18, 847–856,
534 <https://doi.org/10.5194/nhess-18-847-2018>, 2018.
- 535 Scasta, J. D., Weir, J. R., and Stambaugh, M. C.: Droughts and wildfires in western U.S. rangelands, *Rangelands*,
536 38, 197–203, <https://doi.org/10.1016/j.rala.2016.06.003>, 2016.
- 537 Schnell, J. L., Holmes, C. D., Jangam, A., and Prather, M. J.: Skill in forecasting extreme ozone pollution episodes
538 with a global atmospheric chemistry model, *Atmospheric Chem. Phys.*, 14, 7721–7739, <https://doi.org/10.5194/acp-14-7721-2014>, 2014.
- 540 Schroder, J. C., Campuzano-Jost, P., Day, D. A., Shah, V., Larson, K., Sommers, J. M., Sullivan, A. P., Campos, T.,
541 Reeves, J. M., Hills, A., Hornbrook, R. S., Blake, N. J., Scheuer, E., Guo, H., Fibiger, D. L., McDuffie, E. E., Hayes,
542 P. L., Weber, R. J., Dibb, J. E., Apel, E. C., Jaeglé, L., Brown, S. S., Thornton, J. A., and Jimenez, J. L.: Sources and



- 543 secondary production of organic aerosols in the northeastern United States during winter, *J. Geophys. Res.*
544 *Atmospheres*, 123, 7771–7796, <https://doi.org/10.1029/2018JD028475>, 2018.
- 545 Séférian, R., Nabat, P., Michou, M., Saint-Martin, D., Voldoire, A., Colin, J., Decharme, B., Delire, C., Berthet, S.,
546 Chevallier, M., Sénési, S., Franchisteguy, L., Vial, J., Mallet, M., Joetzjer, E., Geoffroy, O., Guérémy, J.-F., Moine,
547 M.-P., Msadek, R., Ribes, A., Rocher, M., Roehrig, R., Salas-y-Méllia, D., Sanchez, E., Terray, L., Valcke, S.,
548 Waldman, R., Aumont, O., Bopp, L., Deshayes, J., Éthé, C., and Madec, G.: Evaluation of CNRM Earth System
549 Model, CNRM-ESM2-1: Role of Earth System Processes in Present-Day and Future Climate, *J. Adv. Model. Earth*
550 *Syst.*, 11, 4182–4227, <https://doi.org/10.1029/2019MS001791>, 2019.
- 551 Seland, Ø., Bentsen, M., Olivie, D., Toniazzo, T., Gjermundsen, A., Graff, L. S., Debernard, J. B., Gupta, A. K., He,
552 Y.-C., Kirkevåg, A., Schwinger, J., Tjiputra, J., Aas, K. S., Bethke, I., Fan, Y., Griesfeller, J., Grini, A., Guo, C.,
553 Ilicak, M., Karset, I. H. H., Landgren, O., Liakka, J., Moseid, K. O., Nummelin, A., Spensberger, C., Tang, H.,
554 Zhang, Z., Heinze, C., Iversen, T., and Schulz, M.: Overview of the Norwegian Earth System Model (NorESM2)
555 and key climate response of CMIP6 DECK, historical, and scenario simulations, *Geosci. Model Dev.*, 13, 6165–
556 6200, <https://doi.org/10.5194/gmd-13-6165-2020>, 2020.
- 557 Senior, C. A., Jones, C. G., Wood, R. A., Sellar, A., Belcher, S., Klein-Tank, A., Sutton, R., Walton, J., Lawrence,
558 B., Andrews, T., and Mulcahy, J. P.: U.K. Community Earth System Modeling for CMIP6, *J. Adv. Model. Earth*
559 *Syst.*, 12, e2019MS002004, <https://doi.org/10.1029/2019MS002004>, 2020.
- 560 Strzepek, K., Yohe, G., Neumann, J., and Boehlert, B.: Characterizing changes in drought risk for the United States
561 from climate change, *Environ. Res. Lett.*, 5, 044012, <https://doi.org/10.1088/1748-9326/5/4/044012>, 2010.
- 562 Surratt, J. D., Chan, A. W. H., Eddingsaas, N. C., Chan, M., Loza, C. L., Kwan, A. J., Hersey, S. P., Flagan, R. C.,
563 Wennberg, P. O., and Seinfeld, J. H.: Reactive intermediates revealed in secondary organic aerosol formation from
564 isoprene, *Proc. Natl. Acad. Sci.*, 107, 6640–6645, <https://doi.org/10.1073/pnas.0911114107>, 2010.
- 565 Tai, A. P. K., Mickley, L. J., and Jacob, D. J.: Correlations between fine particulate matter (PM_{2.5}) and
566 meteorological variables in the United States: Implications for the sensitivity of PM_{2.5} to climate change, *Atmos.*
567 *Environ.*, 44, 3976–3984, <https://doi.org/10.1016/j.atmosenv.2010.06.060>, 2010.
- 568 Tatebe, H., Ogura, T., Nitta, T., Komuro, Y., Ogochi, K., Takemura, T., Sudo, K., Sekiguchi, M., Abe, M., Saito, F.,
569 Chikira, M., Watanabe, S., Mori, M., Hirota, N., Kawatani, Y., Mochizuki, T., Yoshimura, K., Takata, K., O’ishi,
570 R., Yamazaki, D., Suzuki, T., Kurogi, M., Kataoka, T., Watanabe, M., and Kimoto, M.: Description and basic
571 evaluation of simulated mean state, internal variability, and climate sensitivity in MIROC6, *Geosci. Model Dev.*, 12,
572 2727–2765, <https://doi.org/10.5194/gmd-12-2727-2019>, 2019.
- 573 Taufik, M., Torfs, P. J. J. F., Uijlenhoet, R., Jones, P. D., Murdiyarsa, D., and Van Lanen, H. A. J.: Amplification of
574 wildfire area burnt by hydrological drought in the humid tropics, *Nat. Clim. Change*, 7, 428–431,
575 <https://doi.org/10.1038/nclimate3280>, 2017.
- 576 Thornhill, G., Collins, W., Olivie, D., Skeie, R. B., Archibald, A., Bauer, S., Checa-Garcia, R., Fiedler, S., Folberth,
577 G., Gjermundsen, A., Horowitz, L., Lamarque, J.-F., Michou, M., Mulcahy, J., Nabat, P., Naik, V., O’Connor, F.
578 M., Paulot, F., Schulz, M., Scott, C. E., Séférian, R., Smith, C., Takemura, T., Tilmes, S., Tsigaridis, K., and Weber,
579 J.: Climate-driven chemistry and aerosol feedbacks in CMIP6 Earth system models, *Atmospheric Chem. Phys.*, 21,
580 1105–1126, <https://doi.org/10.5194/acp-21-1105-2021>, 2021.
- 581 Tsui, W. G., Woo, J. L., and McNeill, V. F.: Impact of Aerosol-Cloud Cycling on Aqueous Secondary Organic
582 Aerosol Formation, *Atmosphere*, 10, 666, <https://doi.org/10.3390/atmos10110666>, 2019.
- 583 Turnock, S. T., Allen, R. J., Andrews, M., Bauer, S. E., Deushi, M., Emmons, L., Good, P., Horowitz, L., John, J.
584 G., Michou, M., Nabat, P., Naik, V., Neubauer, D., O’Connor, F. M., Olivie, D., Oshima, N., Schulz, M., Sellar, A.,
585 Shim, S., Takemura, T., Tilmes, S., Tsigaridis, K., Wu, T., and Zhang, J.: Historical and future changes in air



- 586 pollutants from CMIP6 models, *Atmospheric Chem. Phys.*, 20, 14547–14579, [https://doi.org/10.5194/acp-20-](https://doi.org/10.5194/acp-20-14547-2020)
587 14547-2020, 2020.
- 588 Vicente-Serrano, S. M., Beguería, S., and López-Moreno, J. I.: A multiscalar drought index sensitive to global
589 warming: The Standardized Precipitation Evapotranspiration Index, *J. Clim.*, 23, 1696–1718,
590 <https://doi.org/10.1175/2009JCLI2909.1>, 2010.
- 591 Wang, Y., Xie, Y., Cai, L., Dong, W., Zhang, Q., and Zhang, L.: Impact of the 2011 southern U.S. drought on
592 ground-level fine aerosol concentration in summertime, *J. Atmospheric Sci.*, 72, 1075–1093,
593 <https://doi.org/10.1175/JAS-D-14-0197.1>, 2015.
- 594 Wang, Y., Xie, Y., Dong, W., Ming, Y., Wang, J., and Shen, L.: Adverse effects of increasing drought on air quality
595 via natural processes, *Atmospheric Chem. Phys.*, 17, 12827–12843, <https://doi.org/10.5194/acp-17-12827-2017>,
596 2017.
- 597 Wang, Y., Wang, J., Wang, Y., and Li, W.: Drought impacts on PM_{2.5} composition and amount over the US during
598 1988–2018, *J. Geophys. Res. Atmospheres*, 127, e2022JD037677, <https://doi.org/10.1029/2022JD037677>, 2022a.
- 599 Wang, Y., Lin, N., Li, W., Guenther, A., Lam, J. C. Y., Tai, A. P. K., Potosnak, M. J., and Seco, R.: Satellite-
600 derived constraints on the effect of drought stress on biogenic isoprene emissions in the southeastern US,
601 *Atmospheric Chem. Phys.*, 22, 14189–14208, <https://doi.org/10.5194/acp-22-14189-2022>, 2022b.
- 602 Wilhite, D. A., Svoboda, M. D., and Hayes, M. J.: Understanding the complex impacts of drought: A key to
603 enhancing drought mitigation and preparedness, *Water Resour. Manag.*, 21, 763–774,
604 <https://doi.org/10.1007/s11269-006-9076-5>, 2007.
- 605 Wu, T., Zhang, F., Zhang, J., Jie, W., Zhang, Y., Wu, F., Li, L., Yan, J., Liu, X., Lu, X., Tan, H., Zhang, L., Wang,
606 J., and Hu, A.: Beijing Climate Center Earth System Model version 1 (BCC-ESM1): model description and
607 evaluation of aerosol simulations, *Geosci. Model Dev.*, 13, 977–1005, <https://doi.org/10.5194/gmd-13-977-2020>,
608 2020.
- 609 Xie, Y., Wang, Y., Dong, W., Wright, J. S., Shen, L., and Zhao, Z.: Evaluating the response of summertime surface
610 sulfate to hydroclimate variations in the continental United States: Role of meteorological inputs in the GEOS-Chem
611 model, *J. Geophys. Res. Atmospheres*, 124, 1662–1679, <https://doi.org/10.1029/2018JD029693>, 2019.
- 612 Xu, L., Guo, H., Boyd, C. M., Klein, M., Bougiatioti, A., Cerully, K. M., Hite, J. R., Isaacman-VanWertz, G.,
613 Kreisberg, N. M., and Knote, C.: Effects of anthropogenic emissions on aerosol formation from isoprene and
614 monoterpenes in the southeastern United States, *Proc. Natl. Acad. Sci.*, 112, 37–42, 2015.
- 615 Yli-Juuti, T., Mielonen, T., Heikkinen, L., Arola, A., Ehn, M., Isokääntä, S., Keskinen, H.-M., Kulmala, M., Laakso,
616 A., Lipponen, A., Luoma, K., Mikkonen, S., Nieminen, T., Paasonen, P., Petäjä, T., Romakkaniemi, S., Tonttila, J.,
617 Kokkola, H., and Virtanen, A.: Significance of the organic aerosol driven climate feedback in the boreal area, *Nat.*
618 *Commun.*, 12, 5637, <https://doi.org/10.1038/s41467-021-25850-7>, 2021.
- 619 Yukimoto, S., Kawai, H., Koshiro, T., Oshima, N., Yoshida, K., Urakawa, S., Tsujino, H., Deushi, M., Tanaka, T.,
620 Hosaka, M., Yabu, S., Yoshimura, H., Shindo, E., Mizuta, R., Obata, A., Adachi, Y., and Ishii, M.: The
621 Meteorological Research Institute Earth System Model Version 2.0, MRI-ESM2.0: Description and Basic
622 Evaluation of the Physical Component, *J. Meteorol. Soc. Jpn. Ser II*, 97, 931–965,
623 <https://doi.org/10.2151/jmsj.2019-051>, 2019.
- 624 Zhang, X., Liu, Z., Hecobian, A., Zheng, M., Frank, N. H., Edgerton, E. S., and Weber, R. J.: Spatial and seasonal
625 variations of fine particle water-soluble organic carbon (WSOC) over the southeastern United States: implications
626 for secondary organic aerosol formation, *Atmospheric Chem. Phys.*, 12, 6593–6607, [https://doi.org/10.5194/acp-12-](https://doi.org/10.5194/acp-12-6593-2012)
627 6593-2012, 2012.

<https://doi.org/10.5194/egusphere-2024-430>

Preprint. Discussion started: 12 March 2024

© Author(s) 2024. CC BY 4.0 License.



628 Zhao, Z., Wang, Y., Qin, M., Hu, Y., Xie, Y., and Russell, A. G.: Drought impacts on secondary organic aerosol: a
629 case study in the southeast United States, *Environ. Sci. Technol.*, 53, 242–250,
630 <https://doi.org/10.1021/acs.est.8b04842>, 2019.

631

632